Phosphorescent Cationic Au_4Ag_2 Alkynyl Cluster Complexes for Efficient Solution-Processed Organic Light-Emitting Diodes

*Liang-Jin Xu, Jin-Yun Wang, Xiao-Feng Zhu, Xian-Chong Zeng, and Zhong-Ning Chen**

Cationic Au_4Ag_2 heterohexanuclear aromatic acetylides cluster complexes supported by bis(2-diphenylphosphinoethyl)phenylphosphine (dpep) are prepared. The Au_4Ag_2 cluster structure originating from the combination of one anionic $[Au(C{\equiv}CR)_2]^-$ with one cationic $[Au_3Ag_2(dpep)_2(C{\equiv}CR)_2]^{3+}$ through the formation of Ag–acetylide η^2-bonds is highly stabilized by Au–Ag and Au–Au contacts. The Au_4Ag_2 alkynyl cluster complexes are moderately phosphorescent in the fluid CH_2Cl_2 solution, but exhibit highly intense phosphorescent emission in solid state and film. As revealed by theoretical computational studies, the phosphorescence is ascribable to significant $^3[\pi$ (aromatic acetylide) $\rightarrow$ s/p (Au)] ^{3}LMCT parentage with a noticeable Au_4Ag_2 cluster centered $^3[d \rightarrow s/p]$ triplet state. Taking advantage of mCP and OXD-7 as a mixed host with 20 wt% dopant of phosphorescent Au_4Ag_2 cluster complex in the emitting layer, solution-processed organic light-emitting diodes (OLEDs) exhibit highly efficient electrophosphorescence with the maximum current, power, and external quantum efficiencies of 24.1 cd A^{-1}, 11.6 lm W^{-1}, and 7.0%, respectively. Introducing copper(I) thiocyanate (CuSCN) as a hole-transporting layer onto the PEDOT:PSS hole-injecting layer through the orthogonal solution process induces an obvious improvement of the device performance with lower turn-on voltage and higher electroluminescent efficiency.

1. Introduction

Owing to their splendid application and industrialization prospect in solid-state lighting and full-color flat-panel display, organic light-emitting diodes (OLEDs) based on phosphorescent neutral metal complexes with iridium(III),[1] platinum(II),[2] osmium(II),[3] gold(III),[4] and copper(I)[5] etc. have been vigorously investigated. Nevertheless, the development of OLEDs based on phosphorescent cationic or anionic metal complexes is still in its infancy.[6–8] In contrast to the vacuum thermal evaporation technique for the fabrication of OLEDs based on luminescent neutral complexes, an inexpensive and convenient solution-processed procedure is usually utilized to prepare OLEDs for ionic metal complexes.[9] Relative to vacuum thermal evaporation deposition, the solution spin-coating process displays several beneficial aspects.[10] (i) The materials can be more efficiently used for solution-processed OLEDs; (ii) solution processing is advantageous for its low-cost and large area manufacturability; (iii) fabrication of multidopant devices such as white-light OLEDs is simple because co-doping of several dopants is easily manipulated by mixing dopants and host materials in solutions.

Compared with neutral metal complexes, ionic metal coordination species take some advantages, including easy preparation under relatively mild conditions, good solubility in organic solvents, high photo- and thermal stability, etc. Nonetheless, electroluminescent performance of solution-processed OLEDs for phosphorescent ionic metal complexes[7,8] is still much lower than that of OLEDs based on neutral iridium(III) and platinum(II) complexes by vacuum thermal evaporation. It is envisioned that the solution-processed approach exhibits huge potential and prosperous prospect to achieve high-performance OLEDs with highly efficient electroluminescence.

Compared with those in mononuclear transition metal complexes, d orbitals in metal polynuclear cluster complexes are more heavily involved in the excited states because of noticeable intermetallic interaction in cluster structures. It is demonstrated that the absorption and emission properties in d^{10}–d^{10} heteronuclear alkynyl cluster complexes are closely correlated to significant d→s/p transition character in the cluster skeletons.[11] The significant participation of d orbitals facilitates spin-forbidden singlet–triplet intersystem crossing and thus results in highly efficient phosphorescence. Nevertheless, the attempt to fabricate OLEDs using metal cluster complexes as phosphorescent emitters has been very limited to date. Ma et al.[12] first made use of the tetranuclear copper(I) complex to fabricate single-layer

L.-J. Xu, Dr. J.-Y. Wang, X.-F. Zhu, X.-C. Zeng, Prof. Z.-N. Chen
State Key Laboratory of Structural Chemistry
Fujian Institute of Research on the Structure of Matter
Chinese Academy of Sciences
Fuzhou, Fujian 350002, China
E-mail: czn@fjirsm.ac.cn
Prof. Z.-N. Chen
State Key Laboratory of Organometallic Chemistry
Shanghai Institute of Organic Chemistry
Chinese Academy of Sciences
Shanghai 200032, China

DOI: 10.1002/adfm.201500060

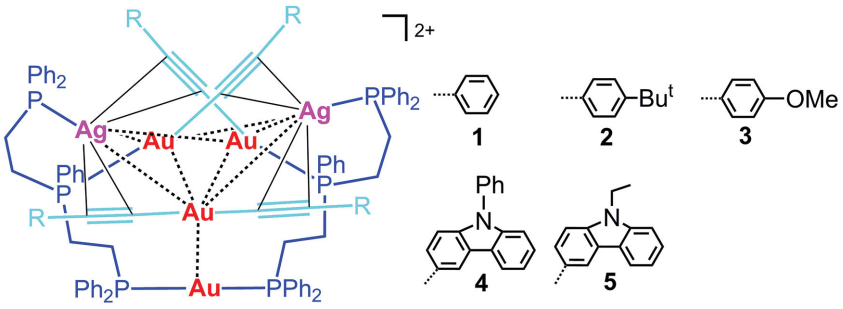

Scheme 1. Au_4Ag_2 alkynyl cluster complexes **1**–**5**.

device ITO/Cu_4:PVK/Al, resulting in inferior electroluminescent performance with the brightness of ≈50 cd m^{-2} and the estimated external quantum efficiency of 0.1%. Recently, Chou and co-workers[13] utilized a tetranuclear gold(I) complex as an emissive dopant and TCTA (TCTA = tris(4-(9*H*-carbazol-9-yl)-phenyl)amine) as a host. Solution-processed OLEDs gave rise to the maximum current, power, and external quantum efficiencies of 6.1 cd A^{-1}, 5.3 lm W^{-1}, and 3.1%, respectively.

In this paper, we describe the use of cationic Au_4Ag_2 heterohexanuclear cluster complexes (**Scheme 1**) as phosphorescent emitters for the fabrication of solution-processed OLEDs. By taking advantage of hole-transporting mCP (mCP = 1,3-di(9*H*-carbazol-9-yl)benzene) and electron-transporting OXD-7 (OXD-7 = 1,3-bis(5-(4-(*tert*-butyl)phenyl)-1,3,4-oxadiazol-2-yl)-benzene) as a mixed host and copper(I) thiocyanate (CuSCN) as a hole-transporting layer through the orthogonal solution spin-coating process, the devices show high performance of electrophosphorescence with the maximum current, power, and external quantum efficiencies of 24.1 cd A^{-1}, 11.6 lm W^{-1}, and 7.0%, respectively. To the best of our knowledge, this represents the best electroluminescent performance for solution-processed OLEDs based on phosphorescent metal cluster complexes.

2. Results and Discussion

2.1. Synthesis and Characterization

Complexes **1**–**5** (Scheme 1) were prepared by suspension of two equiv. polymeric gold(I) aromatic acetylides to CH_2Cl_2 solutions with equimolar dpep and [Ag(tht)](ClO_4), resulting in pale green solutions upon stirring at ambient temperature. The products were purified by silica gel column chromatography with 75–85% yields. The ^{31}P NMR spectra of complexes **1**–**5** exhibited two groups of signals centered at ≈39.5–41.0 and ≈46.0 ppm. The former is ascribed to one terminal P donor of dpep bound to the gold(I) center to form P–Au–P linkage, and the latter is due to the middle P donor of dpep bound to the gold(I) center to afford P–Au–$C_{acetylide}$ linkage. Another set of double of multiplets at 3.2–5.5 ppm arises from the other terminal P donor of dpep bonded to the silver(I) center with significant Ag–P coupling (J_{Ag-P} = 520–540 Hz). The positive ion ESI-MS showed that $[M-ClO_4]^+$ and $[M-2ClO_4]^{2+}$ occurred as base peaks or in high abundance.

The structure of complex **4** was determined by single-crystal X-ray diffraction. The cationic Au_4Ag_2 complex (**Figure 1**) can be viewed as a combination of one anionic $[Au(C{\equiv}CR)_2]^-$ and one cationic $[Au_3Ag_2(dpep)_2(C{\equiv}CR)_2]^{3+}$ through the formation of Ag–acetylide η^2-bonds, as well as Au–Ag and Au–Au interactions between them. The Au–Ag and Au–Au distances are in the range of 2.9724(8)–3.2499(8) and 3.0578(5)–3.1354(6) Å, respectively. These distances are much shorter than the sum of Van der Waals radii for Au–Ag (3.38 Å) and Au–Au (3.32 Å), indicating the presence of substantial d^{10}–d^{10} metallophilic contact within the Au_4Ag_2 cluster core. As depicted in Figure 1, Au4 in anionic $[Au(C{\equiv}CR)_2]^-$ is σ-bonded to two acetylides with a C–Au–C angle of 175.8(3)°. Within cationic $[Au_3Ag_2(dpep)_2(C{\equiv}CR)_2]^{3+}$, Au1 is bound to two P donors with a P–Au–P angle of 169.50(7)°, whereas Au2 and Au3 are coordinated to one P donor and one σ-acetylide C donor with P–Au–C angles of 169.7(3)° and 171.6(2)°, respectively. Both Ag1 and Ag2 centers are bound to one P donor and two η^2 acetylides, affording a distorted trigonal–planar geometry, respectively. The four acetylides adopt $\eta^1(\sigma)$, $\eta^2(\pi)$ coordination mode, bound to gold(I) and silver(I) centers, respectively. The dpep adopts a new bonding fashion, bound to two gold(I) and one silver(I) centers through three P donors.[14]

2.2. Photophysical Properties

The UV–vis spectra of complexes **1**–**5** (**Figure 2**a) display intense absorption peaks at 250–350 nm due to $n{\rightarrow}\pi^*$ and $\pi{\rightarrow}\pi^*$ transitions of dpep and aromatic acetylides. The broad absorption shoulder bands at >350 nm tailing to 470 nm are relevant to charge transfer character and Au_4Ag_2 cluster-centered transition. With the increase of electron-donating capability in the R substituent, the low-energy absorption bands in

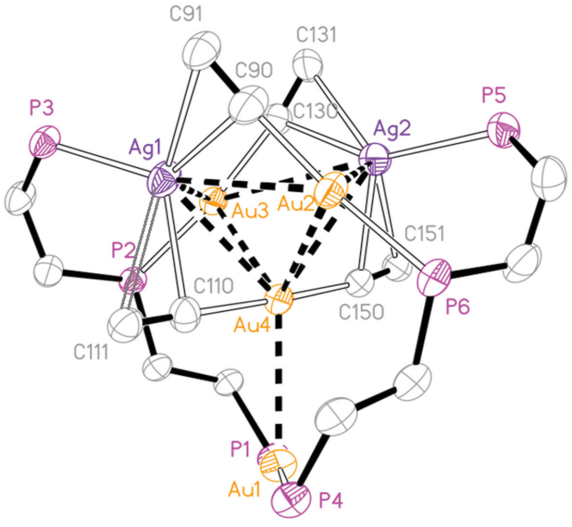

Figure 1. ORTEP drawing (30% thermal ellipsoids) of cationic Au_4Ag_2 cluster complex **4**. 9-Phenylcarbazole groups and phenyl rings on the phosphorus atoms are omitted for clarity.

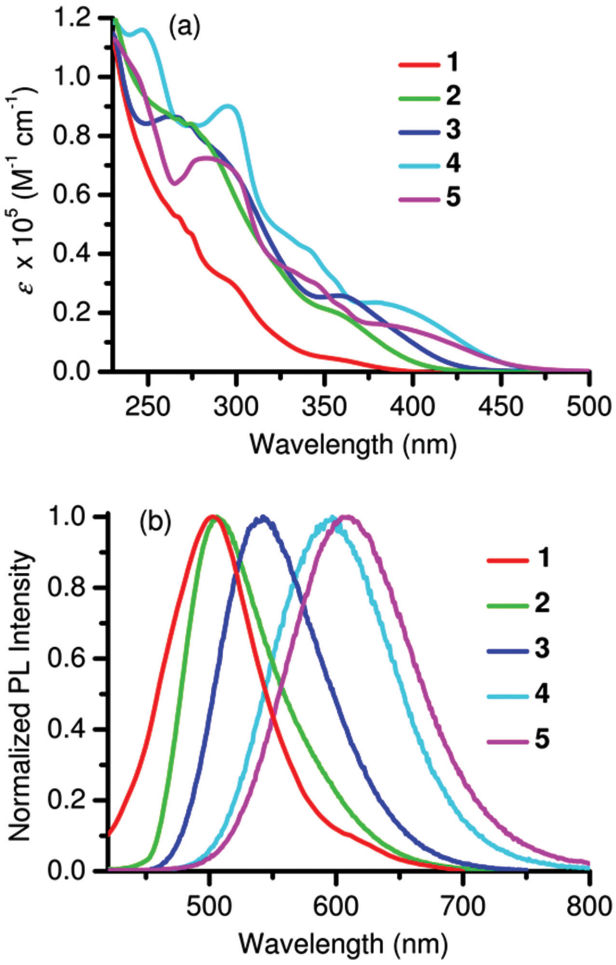

Figure 2. a) UV–vis absorption spectra and b) emission spectra (excitation at 375 nm) of complexes **1**–**5** in CH_2Cl_2 solution (2×10^{-5} M) at ambient temperature.

CH_2Cl_2 display a progressive red-shift following **1** → **2** → **3** → **4** → **5**. This trend coincides well with the gradual reduction of aromatic acetylide→Au LMCT transition energy calculated by TD-DFT computational studies.

Complexes **1**–**5** exhibit bright and long-lived luminescence at ambient temperature with quantum yields of 1.1–10.3% in degassed CH_2Cl_2 solutions. The relatively weak solution phosphorescence is probably ascribed to considerable weak Ag–$C_{acetylide}$ (2.34–2.71 Å) π-bonding that would induce fluxional structures although they could not be resolved in NMR time scale. The microsecond lifetimes together with large Stokes shift imply that the emission is phosphorescent in character with triplet state parentage. As shown in Figure 2b, the emission bands show a progressive red-shift following 502 nm (**1**) → 504 nm (**2**) → 543 nm (**3**) → 592 nm (**4**) → 607 nm (**5**). A substantial dependence of the emission maxima on the electron-donating ability of R substituents in aromatic acetylides is well correlated with the dominant ^{3}LMCT origin mixed with the noticeable cluster-centered ^{3}[d → s/p] triplet excited state.

As shown in **Table 1**, the phosphorescent quantum yields of powder samples (Φ_{em} = 19.8–77.2%) are much higher than those in solutions (Φ_{em} = 1.1–10.3%), indicating that nonradiative deactivation is highly constrained in a solid state. When 20 wt% Au_4Ag_2 species is doped to a CH_2Cl_2 solution with mixed mCP:OXD-7 (53:27 wt%), the films prepared by spin-coating exhibit only the phosphorescent emission that is typical of Au_4Ag_2 cluster complexes without the detection of the emission of mCP and OXD-7 (Figure S4, Supporting Information). It is obvious that the excited state energy of mCP and OXD-7 is effectively transferred to lower lying Au_4Ag_2 species in films. Since the emission bands of mCP and OXD-7 overlap well with the UV–vis absorption spectra of Au_4Ag_2 complexes, the energy transfer is highly facilitated. Although the emission spectra of Au_4Ag_2 species in mCP:OXD-7 doping films display distinct blue-shifts relative to those in solid powder, the phosphorescent quantum yields of Au_4Ag_2 species in the dilute matrix (Table 1) are comparable to those in pure solid samples.

Upon irradiation under UV–vis light, the mCP:OXD-7 film doped with 20 wt% complex **4** keeps integrity without distinct degradation upon monitored by emission spectra and phosphorescent quantum yield. Thermogravimetric analysis for complex **4** (Figure S1, Supporting Information) in atmospheric environment and in the temperature range 20–600 °C shows that it is thermally stable without loss of weight up to 260 °C. Consequently, intense phosphorescence in doped film, high photo- and thermal stability, and good solubility in organic solvents imply that these cationic Au_4Ag_2 complexes can be utilized as viable phosphorescent dopants for solution-processed OLEDs.

2.3. Theoretical Computational Studies

The theoretical computational studies were carried out for compounds **1**–**5** to elucidate the absorption and emission character in singlet and triplet excited states. Triphosphine ligand

Table 1. The emission wavelengths, lifetimes, and quantum yields for Au_4Ag_2 cluster complexes **1**–**5**.

	CH_2Cl_2[a)]			Solid state			mCP:OXD-7:Au_4Ag_2 film (53:27:20 wt%)		
Complex	λ_{em} [nm]	τ_{em} [μs]	Φ_{em} [%]	λ_{em} [nm]	τ_{em} [μs]	Φ_{em} [%]	λ_{em} [nm]	τ_{em} [μs]	Φ_{em} [%]
1	502	6.48	1.1	508	3.63	65.6	485	3.46	21.3
2	504	5.63	2.5	520	1.03	61.7	493	4.57	58.9
3	543	5.20	10.3	542	7.84	77.2	517	7.23	62.5
4	592	12.1	1.7	584	3.63	25.6	533	3.03	53.5
5	607	15.1	9.6	598	4.74	19.8	554	4.27	49.7

[a)]The solution concentration is 2×10^{-5} M and the excitation wavelength is 375 nm.

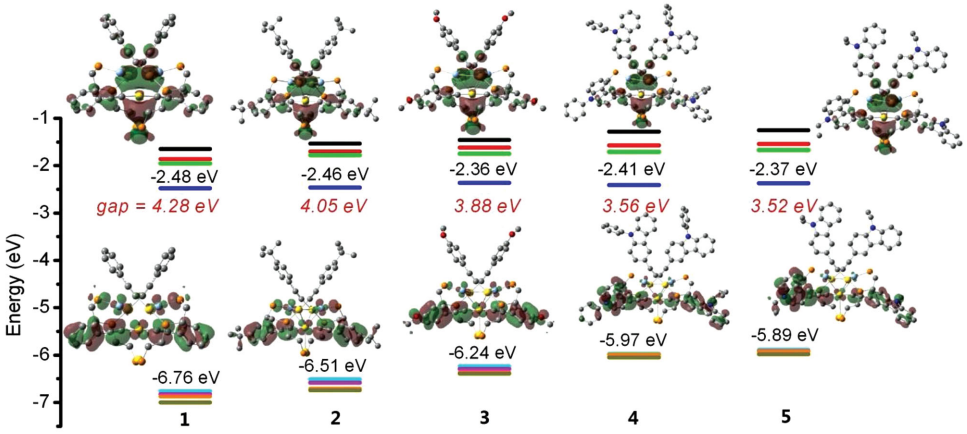

Figure 3. Plots of the HOMOs and LUMOs of complexes **1**–**5** by TD-DFT calculation at the PBE1PBE level (isovalue = 0.025).

is simplified as $HP(C_2H_4PH_2)_2$ to save calculational time. The plots of HOMO and LUMO and their energy level diagrams are depicted in **Figure 3**. The molecular orbital compositions involved in singlet states and lowest triplet states together with the absorption and emission transition character calculated by the TD-DFT method at the PBE1PBE level are summarized in **Tables 2** and **3** for complex **1**, and provided as Supporting Information for compounds **2**–**5** (Tables S3–S12, Supporting Information).

The HOMO is mainly resident on aromatic acetylides with moderate distribution on the Au_4Ag_2 cluster core. The LUMO focuses primarily on Au centers with mixed

Table 2. The partial molecular orbital composition (%) by SCPA approach (C-squared population analysis proposed by Ros and Schuit) and the absorption transition for Au_4Ag_2 Complex **1** in dichloromethane by TD-DFT method at the PBE1PBE level.

Orbital	Energy [eV]	MO contribution [%]			
		Ag (s/p/d)	Au (s/p/d)	$HP(C_2H_4PH_2)_2$	$C{\equiv}CC_6H_5$
LUMO+6	–1.09	31.13 (79/20/1)	46.76 (38/59/3)	11.78	10.34
LUMO+3	–1.65	29.79 (73/25/2)	50.18 (90/8/2)	10.60	9.43
LUMO+2	–1.86	10.28 (56/34/10)	48.96 (25/70/5)	18.66	22.10
LUMO+1	–1.95	10.69 (70/16/14)	34.01 (29/67/4)	31.11	24.20
LUMO	–2.48	5.24 (64/27/9)	69.78 (49/47/4)	12.97	12.02
HOMO	–6.76	20.05 (18/8/74)	13.94 (13/12/75)	14.71	51.30
HOMO-1	–6.82	10.18 (24/3/73)	30.60 (37/17/46)	12.19	47.03
HOMO-2	–6.87	14.12 (19/25/56)	39.22 (45/4/51)	4.09	42.47
HOMO-3	–7.00	19.30 (26/17/57)	8.96 (1/21/77)	3.54	68.20
HOMO-5	–7.36	22.04 (17/2/82)	36.77 (49/1/50)	17.02	24.17
HOMO-6	–7.67	24.64 (7/9/84)	23.10 (28/9/63)	20.38	31.89

State	*E*/nm [eV]	O.S.	Transition	Contribution	Assignment	Measured [nm]
S_2	353 (3.52)	0.0611	HOMO→LUMO	49%	^{1}LMCT/^{1}MC	355
			HOMO-1→LUMO	47%	^{1}MC/^{1}LMCT	
S_3	340 (3.64)	0.1922	HOMO-2→LUMO	95%	^{1}MC/^{1}LMCT	
S_{10}	299 (4.15)	0.3292	HOMO-2→LUMO+1	49%	^{1}MC/^{1}IL/^{1}LLCT/^{1}MLCT	300
			HOMO-1→LUMO+2	30%	^{1}MC/^{1}IL/^{1}LMCT	
S_{14}	287 (4.33)	0.1746	HOMO-3→LUMO+1	57%	^{1}MC/^{1}LLCT/^{1}IL/^{1}LMCT	282
			HOMO-6→LUMO	22%	^{1}MC/^{1}LMCT/^{1}IL	
S_{16}	281 (4.41)	0.1791	HOMO-1→LUMO+3	24%	^{1}MC/^{1}LMCT/^{1}IL	
			HOMO-3→LUMO+2	21%	^{1}LMCT/^{1}MC/^{1}LLCT	
			HOMO-2→LUMO+3	18%	^{1}MC/^{1}LMCT	
			HOMO-5→LUMO+1	15%	^{1}MC/^{1}IL/^{1}MLCT	

Table 3. Partial molecular orbital composition (%) in the lowest triplet state and the emission transition for complex **1** in dichloromethane by the TD-DFT method at the PBE1PBE level.

Orbital	Energy [eV]	MO contribution [%]				
		Ag (s/p/d)	Au (s/p/d)	$HP(C_2H_4PH_2)_2$	$C{\equiv}CC_6H_5$	
LUMO	–2.97	10.14 (71/25/4)	62.26 (51/44/5)	13.67	13.93	
HOMO	–6.42	18.83 (33/17/50)	13.47 (17/7/76)	8.14	59.56	
States	*E*/nm [eV]	O.S.	Transition	Contribution	Assignment	Measured [nm]
T_1	555 (2.23)	0.0000	HOMO→LUMO	80%	^{3}LMCT/^{3}MC	502

s/p orbital composition. The low-energy absorption due to HOMO→LUMO thus exhibits significant [π (acetylide) → s/p (Au)] LMCT (ligand-to-metal charge transfer) parentage and moderate Au_4Ag_2 cluster-centerd [d → s/p] character.

The HOMO and LUMO character in the triplet state (Table 2) is comparable to that in the singlet state (Table 1). The phosphorescence originates largely from the ^{3}[π (acetylide) → s/p (Au)] ^{3}LMCT triplet excited state with a noticeable cluster-centered ^{3}[d → s/p] character. It is worthy to note that relative to complexes **1**–**3** with $C{\equiv}CC_6H_4R$-4 (R = H, Bu^t, OMe), complexes **4** and **5** with carbazole–acetylides show more LMCT state and less Au_4Ag_2 cluster-centered character. It appears that the carbazole group makes a distinct contribution to the excited state and transition character. As depicted in Figure 3, while the LUMO level keeps almost constant, the HOMO level shows gradual ascent following –6.76 eV (**1**) → –6.51 eV (**2**) → –6.24 eV (**3**) → –5.97 eV (**4**) → –5.89 eV (**5**) so that the HOMO–LUMO gap is progressively reduced following 4.28 eV (**1**) → 4.05 eV (**2**) → 3.88 eV (**3**) → 3.56 eV (**4**) → 3.52 eV (**5**). Such a trend is in accordance with a gradual red-shift of the phosphorescence emission in fluid CH_2Cl_2 following 502 nm (**1**) → 504 nm (**2**) → 543 nm (**3**) → 592 nm (**4**) → 607 nm (**5**).

2.4. Electrophosphorescence

Electroluminescence performance of OLEDs based on the phosphorescent Au_4Ag_2 cluster complexes **1**–**5** was investigated using device configuration ITO/PEDOT:PSS (50 nm)/host:Au_4Ag_2 complex (50 nm)/TPBi (50 nm)/LiF (1 nm)/Al (100 nm). The structures of organic materials and energy level diagrams in OLEDs are depicted in **Scheme 2**. The optimization procedure of the performance of OLEDs based on complex **4** is summarized in **Table 4**. The optimized electroluminescent data of solution-processed OLEDs for complexes **1**–**5** are shown in **Table 5**.

The poly(3,4-ethylenedioxythiophene):poly(styrenesulfonate) (PEDOT:PSS) was used as a hole-injection layer, TPBi as an

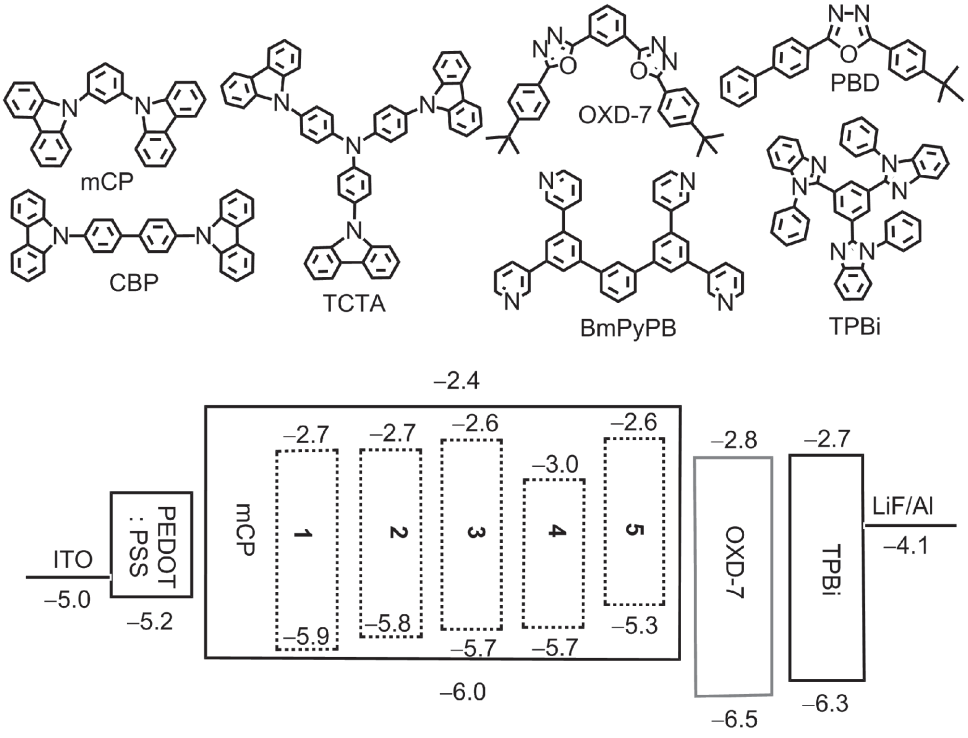

Scheme 2. The organic materials and energy level diagrams in OLEDs. The HOMO and LUMO levels of complexes **1**–**5** were estimated by X-ray photoelectron spectra and optical band gaps.

Table 4. Optimization of electroluminescent performance of OLEDs based on complex **4** by modifying host and doping concentration in emissive layer, as well as electron-transporting layer (ETL).

Device	Host	ETL	Doping [%]	V_{on} [V]	L_{max} [cd m^{-2}]	CE_{max} [cd A^{-1}]	PE_{max} [lm W^{-1}]	EQE [%]	λ_{max} [nm]
1	CBP	TPBi	20	7.4	8697	5.4	1.7	1.7	532
2	TCTA	TPBi	20	6.0	3021	5.9	2.4	1.9	532
3	mCP	TPBi	20	6.6	12 591	7.0	2.1	2.6	532
4	CBP : OXD-7 (53%:27%)	TPBi	20	8.4	17 635	18.0	4.4	5.1	537
5	TCTA:OXD-7 (53%:27%)	TPBi	20	8.0	6136	14.3	3.9	4.0	538
6	mCP:PBD (53%:27%)	TPBi	20	7.0	14 274	12.5	4.1	3.9	532
7	mCP:TPBi (53%:27%)	TPBi	20	9.1	17 643	17.2	4	4.9	534
8	mCP:BmPyPb (53%:27%)	TPBi	20	7.2	9518	10.9	3.5	3.2	533
9	mCP:OXD-7 (60%:30%)	TPBi	10	7.8	17 605	16.9	4.3	5.0	532
10	mCP:OXD-7 (57%:28%)	TPBi	15	7.9	17 651	20.5	5.7	6.1	532
11	mCP:OXD-7 (53%:27%)	TPBi	20	7.5	17 662	22.5	6.5	6.8	537
12	mCP:OXD-7 (50%:25%)	TPBi	25	10.6	13 837	12.9	2.4	3.8	532
13	mCP:OXD-7 (53%:27%)	OXD-7	20	12.2	3957	13.0	2.3	4.3	547
14	mCP:OXD-7 (53%:27%)	PBD	20	7.2	10 097	14.6	4.2	4.3	549
15	mCP:OXD-7 (53%:27%)	BmPyPb	20	8.1	12 691	21.8	5.6	6.5	549

electron-transporting layer, and LiF as an electron-injecting layer. A hole-transporting-type host and an electron-transporting-type host were utilized as mixed host materials. The use of a mixed host with a hole-transporting-type host blended to another electron-transporting-type host is in favor of injecting holes and electrons in the emitting layer so that carrier balance is readily attained by simply adjusting the composition of mixed host materials.[15] Using mixed host instead of single host is also advantageous in that the molecular packing of the host and the dopant can be hindered due to intermixing of two host materials with phosphorescent emitter, which is favorable for the formation of uniform films with superior quality. Additionally, an exciplex-forming co-host in an emitting layer can also achieve low efficiency roll-off because it is presumed to give a broad emission zone to reduce the triplet and polaron density and protect them from accumulating in a narrow zone in an emitting layer.[16]

Table 5. The performance data of OLEDs based on phosphorescent Au_4Ag_2 cluster complexes **1**–**5**.

Compound	λ_{EL} [nm]	V_{on} [V][a)]	L_{max} [cd m^{-2}][b)]	CE_{max} [cd A^{-1}] [c)]	PE_{max} [lm W^{-1}][d)]	EQE_{max} [%][e)]
1	482	6.6	7981	7.9	2.7	3.9
2	490	6.7	6468	12.1	4.0	5.3
3	518	8.4	17160	21.8	5.6	6.5
4	537	7.5	17662	22.5	6.5	6.8
	539 [f)]	4.6	8804	24.1	11.6	7.0
5	550	7.7	17651	20.9	6.0	6.1

[a)]Turn-on voltage at 1 cd m^{-2}; [b)]Maximum luminance; [c)]Maximum current efficiency; [d)]Maximum power efficiency; [e)]Maximum external quantum efficiency; [f)]Based on device configuration ITO/PEDOT:PSS (50 nm)/CuSCN (30 nm)/mCP (53.6%):OXD-7 (26.4%):20.0% wt Au_4Ag_2 complex (50 nm)/TPBi (50 nm)/LiF (1 nm)/Al (100 nm).

Using complex **4** as a phosphorescent dopant in an emitting layer, the devices were optimized by modifying host and doping percentage between the host and the dopant. As shown in Table 4, mCP as a single host gave better performance than that of CBP or TCTA because of the higher triplet energy of mCP (2.90 eV) than that of CBP (2.60 eV) and TCTA (2.70 eV)[15,17] and thus more facile energy transfer to phosphorescent dopant for mCP, but none of mCP, CBP, or TCTA as a single host afforded superior electroluminescent performance. Instead, mixed host consisting of a hole-transporting-type host and an electron-transporting-type host brought about much higher electrophosphorescent efficiency. In particular, the use of hole-transporting mCP and electron-transporting OXD-7 in a 2:1 weight ratio as a mixed host results in superior device performance. By adjusting doping concentration in the emitting layer, it is demonstrated that doping 20% Au_4Ag_2 species to mixed host of mCP:OXD-7 (53%:27%) resulted in the highest electroluminescent efficiency. The devices were also optimized by changing the electron-transporting layer. Of the four electron-transporting materials such as OXD-7, PBD, TPBi, and BmPyPb, TPBi gave rise to the best performance of devices as an electron-transporting/hole-blocking layer.

By taking advantage of device configuration ITO/PEDOT:PSS (50 nm)/mCP (53.6%):OXD-7 (26.4%):20.0% wt Au_4Ag_2 complex (50 nm)/TPBi (50 nm)/LiF (1 nm)/Al (100 nm), the maximum current (CE) and external quantum (EQE) efficiencies (Table 5) of the devices are 21.8 cd A^{-1} and 6.5% for complex **3**, 22.5 cd A^{-1} and 6.8% for complex **4**, and 20.9 cd A^{-1} and 6.1% for complex **5**. As depicted in **Figure 4**a, the electroluminescence spectra of OLEDs based on complexes **1**–**5** accord well with the corresponding phosphorescent emission spectra of mCP:OXD-7:Au_4Ag_2 complex films without distinct interference from organic materials. With the increase of electron-donating ability of R groups in aromatic acetylides, the maxima of electroluminescent spectra show gradual red-shifts

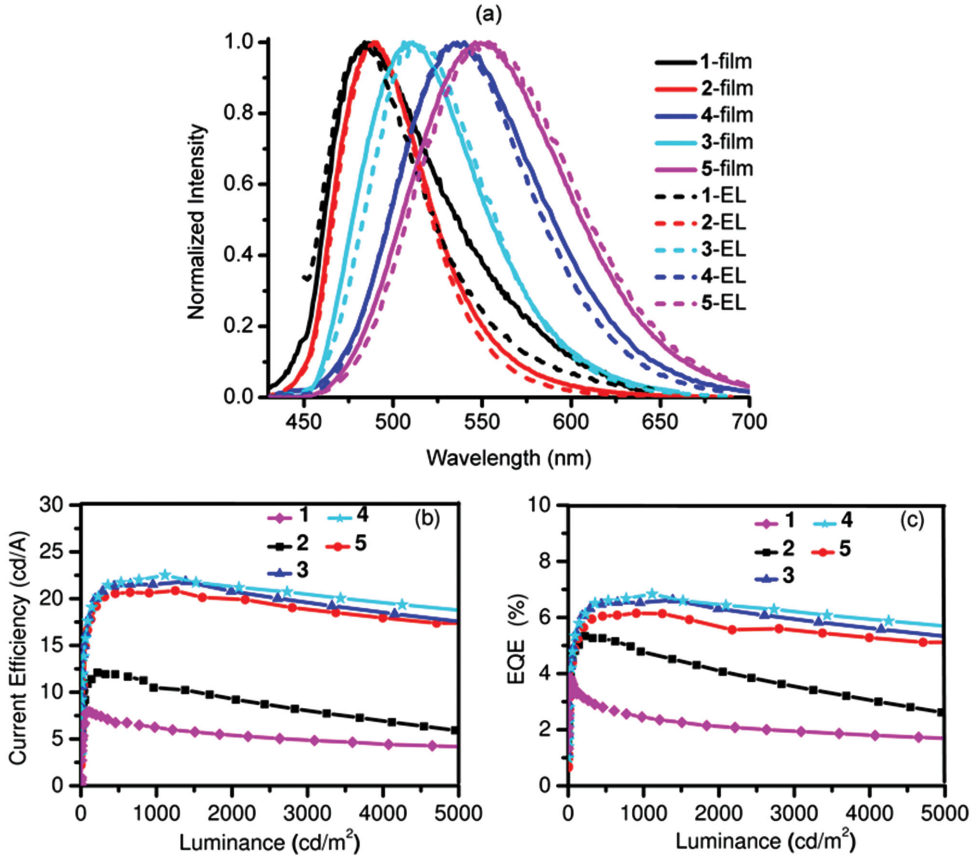

Figure 4. a) Comparison of phosphorescent emission spectra of mCP:OXD-7:Au_4Ag_2 complex films (solid) and electroluminescent spectra of OLEDs (dashed) based on complexes **1**–**5**. b) Current efficiency versus luminance for electroluminescent devices based on complexes **1**–**5**. c) External quantum efficiency (EQE) versus luminance for electroluminescent devices based on complexes **1**–**5**.

following 482 nm (**1**) → 490 nm (**2**) → 518 nm (**3**) → 537 nm (**4**) → 550 nm (**5**). As a result, electroluminescent colors are successfully modulated by modifying the substituents of aromatic acetylides in complexes **1**–**5**.

As depicted in Figure 4b,c, the current and external quantum efficiencies enhance first and then reduce gradually with the increase of the luminance. The largest current and external quantum efficiencies occur at the luminance of 30250 cd m^{-2} for electroluminescent devices based on complexes **1** and **2**. By contrast, the devices based on complexes **3**, **4**, and **5** exhibit the highest electroluminescent efficiency at the brightness of 1000–1500 cd m^{-2}, a desired performance for flat panel display and lighting.

When CuSCN in diethyl sulfide is orthogonally spin-coated onto the water-soluble PEDOT:PSS hole-injecting layer to serve as a hole-transporting layer,[18] the performance of OLEDs based on complex **4** is further improved (**Figure 5**). With device architecture ITO/PEDOT:PSS (50 nm)/CuSCN (30 nm)/mCP (53.6%):OXD-7 (26.4%):20.0% Au_4Ag_2 complex (50 nm)/TPBi (50 nm)/LiF (1 nm)/Al (100 nm), turn-on voltage at 1 cd m^{-2} is reduced to 4.6 V. The devices show superior performance with current, power, and external quantum efficiencies of 21.7 cd A^{-1}, 11.6 lm W^{-1}, and 6.3% at 100 cd m^{-2}, and 21.5 cd A^{-1}, 9.4 lm W^{-1} and 6.2% at 1000 cd m^{-2}. Obviously, the efficiency roll-off is considerably slow in display relevant luminance range from 100 to 1000 cd m^{-2}. The maximum current, power, and external quantum efficiencies are increased to 24.1 cd A^{-1}, 11.6 lm W^{-1}, and 7.0% in comparison with those of CuSCN-free devices (22.5 cd A^{-1}, 6.5 lm W^{-1}, and 6.8%). The distinct improvement of device performance is attributable to efficient hole-transporting, electron-blocking, and better charge-carrier balance associated with the use of CuSCN because energy barrier from the hole-transporting layer to emitting layer is small (Figure 5c) due to deep valence band (–5.5 eV) of CuSCN.[18b,c] The high-lying conduction band (–1.8 eV) of CuSCN is also favorable for restricting excitons within the emitting layer.

3. Conclusion

The reaction of dpep, [Ag(tht)](ClO_4), and polymeric gold(I) aromatic acetylides resulted in the isolation of cationic Au_4Ag_2 heterohexanuclear cluster complexes. The Au_4Ag_2 cluster structure is composed of one anionic $[Au(C{\equiv}CR)_2]^-$ and one cationic $[Au_3Ag_2(dpep)_2(C{\equiv}CR)_2]^{3+}$ incorporating through the formation of silver–acetylide bonds in η^2 (C≡C) mode, as well as significant Au–Ag interaction. The cationic Au_4Ag_2 heterohexanuclear cluster complexes are moderately phosphorescent in solutions, but show intense phosphorescence in solid state and film. TD-DFT computational studies indicate that the

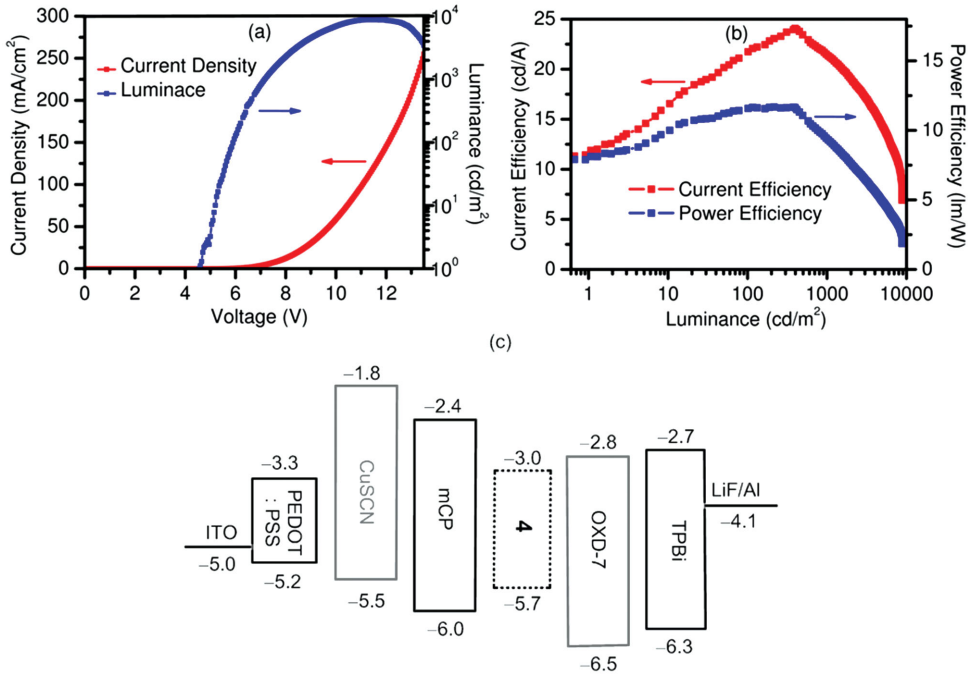

Figure 5. a) Current density–voltage–luminance (*J*–*V*–*L*) characteristics, b) current efficiency/external quantum efficiency versus luminance, and c) energy level diagrams for OLEDs based on complex **4**. The device configuration is ITO/PEDOT:PSS (50 nm)/CuSCN (30 nm)/mCP (53.6%):OXD-7 (26.4%):20.0% Au_4Ag_2 complex (50 nm)/TPBi (50 nm)/LiF (1 nm)/Al (100 nm).

phosphorescence originates from dominant ^{3}LMCT transition together with the noticeable metal cluster centered ^{3}[d→s/p] state. In view of highly efficient phosphorescence in doped film, high thermal and photochemical stability, and excellent solubility in organic solvents, cationic Au_4Ag_2 cluster complexes were utilized as phosphorescent dopants for solution-processed OLEDs. The electrophosphorescent spectra coincide with the phosphorescence emission bands of complexes **1**–**5**. By modifying the substituents in aromatic acetylides, high performance of cyan, green, yellow-green, and yellow electrophosphorescence is successfully achieved. With hole-transporting-type host mCP and electron-transporting host OXD-7 as mixed host, the highest current, powder, and external quantum efficiencies are 24.1 cd A^{-1}, 11.6 lm w^{-1}, and 7.0% for electroluminescent devices using p-type semiconductor CuSCN as a hole-transporting layer.

4. Experimental Section

General Procedures and Materials: All manipulations were conducted under a dry argon atmosphere using Schlenk techniques and vacuum-line systems unless otherwise specified. The solvents were dried, distilled, and degassed prior to use, except that those for spectroscopic measurements were of spectroscopic grade. Bis(2-diphenylphosphinoethyl)phenylphosphine (dpep) was available commercially (Sigma-Aldrich). 3-Ethynyl-9-ethylcarbazole (HC≡C-3-Etcar-9) and 3-ethynyl-9-phenylcarbazole (HC≡C-3-Phcar-9) were prepared by the reaction of 3-bromo-9-ethylcarbazole or 3-bromo-9-phenylcarbazole with ethynyltrimethylsilane in the presence of $Pd(PPh_3)_2Cl_2$ and CuI. Polymeric gold(I) acetylide complexes with various aromatic acetylides were prepared by the similar procedure to that of $\{Au(C{\equiv}CPh)\}_n$.[19] Other reagents were purchased from commercial sources and used as received unless stated otherwise.

$[Au_4Ag_2(dpep)_2(C{\equiv}CC_6H_5)_4](ClO_4)_2$ (***1***): To a CH_2Cl_2 (20 mL) solution of dpep (53.4 mg, 0.1 mmol) was added [Ag(tht)](ClO_4) (29.6 mg, 0.1 mmol) with stirring for 30 min. Upon the addition of $\{Au(C{\equiv}CPh)\}_n$ (59.6 mg, 0.2 mmol), the suspension was stirred at ambient temperature for 2 h, giving a pale green solution. The concentrated solution was chromatographed on a silica gel column using CH_2Cl_2–MeCN (8:1) as an eluent to afford the product as a green solid. Yield: 85%. Anal. Calcd for $C_{100}H_{86}Cl_2O_8P_6Ag_2Au_4{\cdot}3/2CH_2Cl_2$: C, 43.48; H, 3.20. Found: C, 43.41; H, 3.36. ESI-MS *m*/*z* (%): 2576.2 (100) $[M{-}ClO_4]^+$, 1239.0 (8) $[M{-}2ClO_4]^{2+}$. ^{1}H NMR (400 MHz, $CDCl_3$, *δ*): 8.07–7.98 (m, 4H), 7.67–7.53 (m, 18H) 7.51–7.47 (m, 4H), 7.45–7.37 (m, 6H), 7.27–7.23 (m, 4H), 7.20–7.16 (m, 6H), 7.14–7.04 (m, 16H), 6.93–6.84 (m, 8H), 6.82–6.75 (t, 4H), 3.60–3.33 (m, 8H), and 3.31–3.02 (m, 8H). ^{31}P NMR (162 MHz, $CDCl_3$, *δ*): 46.1 (m, 2P), 39.9 (m, 2P), and 4.4 (m, 2P, J_{Ag-P} = 534 Hz). IR (KBr): *ν* = 2059(w), 1112(s).

$[Au_4Ag_2(dpep)_2(C{\equiv}CC_6H_4Bu^t\text{-}4)_4](ClO_4)_2$ (***2***): This compound was prepared by the same synthetic procedure as that of **1**, except for using 1-ethynyl-4-*tert*-butylbenzene instead of phenylacetylene. Yield: 83%. Anal. Calcd for $C_{116}H_{118}Cl_2O_8P_6Ag_2Au_4{\cdot}CH_2Cl_2$: C, 47.07; H, 4.05. Found: C, 47.02; H, 4.09. ESI-MS *m*/*z* (%): 2800.4 (100) $[M{-}ClO_4]^+$, 1351.2 (7) $[M{-}2ClO_4]^{2+}$. ^{1}H NMR (400 MHz, $CDCl_3$, *δ*): 8.11–8.02 (m, 4H), 7.67–7.55 (m, 18H), 7.48–7.40 (m, 12H), 7.38–7.34 (m, 4H), 7.15–6.99 (d, 16H), 6.90–6.81 (m, 8H), 3.60–3.31 (m, 8H), 3.29–3.00 (m, 8H), and 0.02 (s, 36H). ^{31}P NMR (162 MHz, $CDCl_3$, *δ*): 45.9 (m, 2P), 39.5 (m, 2P), 3.2 (m, 2P, J_{Ag-P} = 531 Hz). IR (KBr): *ν* = 2046(w), 1092(s).

$[Au_4Ag_2(dpep)_2(C{\equiv}CC_6H_4OMe\text{-}4)_4](ClO_4)_2$ (***3***): This compound was prepared by the same synthetic procedure as that of **1**, except for the use of 1-ethynyl-4-methoxybenzene instead of phenylacetylene. Yield: 80%. Anal. Calcd for $C_{104}H_{94}Cl_2O_{12}P_6Ag_2Au_4{\cdot}CH_2Cl_2$: C, 43.77; H, 3.36. Found: C, 43.95; H, 3.51. ESI-MS *m*/*z* (%): 2696.2 (100) $[M{-}ClO_4]^+$, 1299.3(5) $[M{-}2ClO_4]^{2+}$. ^{1}H NMR (400 MHz, $CDCl_3$, *δ*): 8.10–8.0 (m, 4H), 7.65–7.55 (m, 18H), 7.53–7.47 (m, 4H), 7.43–7.35 (m, 6H), 7.23–7.18 (d, 4H), 7.15–7.05 (m, 16H), 6.95–6.80 (m, 10H), 6.65–6.60 (d, 4H), 6.39–6.35 (d, 4H), 3.87 (s, 6H), 3.67 (s, 6H), 3.60–3.40 (m, 8H), and 3.21–3.0 (m, 8H). ^{31}P NMR (162 MHz, $CDCl_3$, *δ*): 45.9 (m, 2P), 40.9 (m, 2P), 4.4 (m, 2P, J_{Ag-P} = 531 Hz). IR (KBr): *ν* = 2082(w), 1097(s).

$[Au_4Ag_2$ (dpep)$_2$(C≡C-3-Phcarb-9)$_4](ClO_4)_2$ (**4**): This compound was prepared by the same synthetic procedure as that of **1**, except for using 3-ethynyl-9-phenylcarbazole instead of phenylacetylene. Yield: 85%. Anal. Calcd for $C_{148}H_{114}Cl_2N_4O_8P_6Ag_2Au_4{\cdot}CH_2Cl_2$:C, 52.30; H, 3.42. Found: C, 52.35; H, 3.54. ESI-MS *m/z* (%): 3236.6 (100) $[M–ClO_4]^+$, 1569.4 (40) $[M–2ClO_4]^{2+}$. ^{1}H NMR (400 MHz, $CDCl_3$, δ): 8.20–8.13 (m, 4H), 7.73–7.67 (d, 4H), 7.66–7.60 (m, 18H), 7.59–7.50 (m, 22H), 7.48–7.37 (m, 14H), 7.36–7.30 (m, 12H), 7.18–7.15 (d, 2H), 7.00–6.93 (m, 6H), 6.90–6.75 (m, 12H), 6.38–6.25 (m, 6H), 3.80–3.55 (m, 8H), and 3.15–3.00 (m, 8H). ^{31}P NMR (162 MHz, $CDCl_3$, δ): 46.0 (m, 2P), 41.0 (m, 2P), 3.9 (m, 2P, $J_{Ag–P}$ = 528 Hz). IR (KBr): ν = 2064(w), 1108(s).

$[Au_4Ag_2$ (dpep)$_2$(C≡C-3-Etcarb-9)$_4](ClO_4)_2$ (**5**): This compound was prepared by the same synthetic procedure as that of **1**, except for using 3-ethynyl-9-ethylcarbazole instead of phenylacetylene. Yield: 75%. Anal. Calcd for $C_{132}H_{114}Cl_2N_4O_8P_6Ag_2Au_4{\cdot}2CH_2Cl_2$: C, 48.56; H, 3.59; N, 1.69. Found: C, 48.51; H, 3.72; N, 1.45. ESI-MS *m/z* (%): 3044.3 (100) $[M–ClO_4]^+$, 1474.2 (65) $[M–2ClO_4]^{2+}$. ^{1}H NMR (400 MHz, $CDCl_3$, δ): 8.20–8.12 (m, 4H), 7.70–7.56 (m, 22H), 7.55–7.50 (m, 10H), 7.46–7.31 (m, 22H), 6.97–6.82 (m, 10H), 6.80–6.70 (d, 6H), 6.30–6.23 (m, 4H), 4.50–4.42 (m, 4H), 4.22–4.10 (m, 4H), 3.82–3.45 (m, 8H), 3.35–3.10 (m, 8H), 1.56–1.50 (t, 6H), and 1.34–1.20 (t, 6H). ^{31}P NMR (162 MHz, $CDCl_3$, δ): 45.8 (m, 2P), 41.3 (m, 2P), 4.0 (m, 2P, $J_{Ag–P}$ = 522 Hz). IR (KBr): ν = 2088(w), 1091(s).

Physical Measurements: UV–vis absorption spectra were measured on a Perkin-Elmer Lambda 35 UV–vis spectrophotometer. Infrared spectra (IR) were recorded on a Magna 750 FT-IR spectrophotometer with KBr pellets. Elemental analysis (C, H, N) were carried out on a Perkin-Elmer model 240 C elemental analyzer. ^{1}H NMR and ^{31}P NMR spectra were measured on a Bruker Avance 400 (400 MHz) spectrometer with $SiMe_4$ as the internal reference and H_3PO_4 as the external reference, respectively. Electrospray ionization mass spectrometry (ESI-MS) was performed on a Finnigan LCQ mass spectrometer using dichloromethane and methanol mixtures as mobile phases. The emission and excitation spectra, together with the emissive lifetimes in solid states and degassed solutions, were measured on the Edinburgh FLS920 fluorescence spectrometer. The emission quantum yield (Φ_{em}) in the degassed dichloromethane solution at room temperature was calculated by $\Phi_s = \Phi_r(B_r/B_s)(n_s/n_r)^2(D_s/D_r)$ using $[Ru(bpy)_3](PF_6)_2$ in acetonitrile as the standard (Φ_{em} = 0.062)[20] where the subscripts r and s denote reference standard and the sample solution, respectively, and *n*, *D*, and Φ are the refractive index of the solvents, the integrated intensity, and the luminescence quantum yield, respectively. The quantity *B* is calculated by $B = 1–10^{-AL}$, where *A* is the absorbance at the excitation wavelength and *L* is the optical path length. The solid-state quantum yields of powder samples in sealed quartz cuvettes and films spin-coated in quartz substrates were determined by the integrating sphere (142 mm in diameter) using Edinburgh FLS920 Spectrofluorophotometer.

Crystal Structural Determination: Data collection was performed on Mercury CCD diffractometer by the ω scan technique at room temperature using graphite-monochromated Mo–Ka (λ = 0.71073 Å) radiation. The CrystalClear software package was used for data reduction and empirical absorption correction. The structures were solved by direct methods. The heavy atoms were located from E-map, and the rest of the non-hydrogen atoms were found in subsequent Fourier maps. All non-hydrogen atoms were refined anisotropically, whereas the hydrogen atoms were generated geometrically and refined with isotropic thermal parameters. The structures were refined on F^2 by full-matrix least-squares methods using the *SHELXTL*-97 program package.[21] [CCDC 1041966 (compound **4**) contains the supplementary crystallographic data for this paper. These data can be obtained free of charge from The Cambridge Crystallographic Data Centre via www.ccdc.cam.ac.uk/data_request/cif.].

Device Fabrication and Characterization: ITO substrates were cleaned by sonication in deionized water, acetone, and isopropanol followed by UV-ozone treatment for 15 min. PEDOT:PSS was filtered through a 0.22 μm filter and spin-coated (at 3000 rpm) on the precleaned substrates, and dried at 140 °C for 20 min to give a film of 50 nm thickness. The emitting layer was then overlaid by spin-coating (at 1500 rpm) using a filtered CH_2Cl_2 solution (5.5 mg mL^{-1}) with mixed host materials and Au_4Ag_2 cluster complex. Subsequently, 50 nm of TPBi, 1 nm of LiF, and 100 nm of Al were thermally deposited in an inert chamber at a base pressure less than 4 ×10^{-4} Pa. For device configuration ITO/PEDOT:PSS (50 nm)/CuSCN (30 nm)/mCP (53.6%):OXD-7 (26.4%):20.0% Au_4Ag_2 complex **4** (50 nm)/TPBi (50 nm)/LiF (1 nm)/Al (100 nm), CuSCN dissolved in diethyl sulfide at a concentration of 10 mg mL^{-1} was spin-coated (at 4400 rmp) onto the PEDOT:PSS hole-injecting layer and then annealed at 140 °C for 10 min to achieve a 30 nm thick film. The electroluminescence (EL) spectra were recorded on a HORIBA Jobin-Yvon FluoroMax-4 spectrometer. The current density–voltage–brightness (*I–V–B*) curves of the devices were recorded on a Keithley 2400/2000 source meter and a calibrated silicon photodiode. All measurements of the devices were carried out at room temperature under ambient conditions.

Theoretical Methodology: To understand the electronic and spectroscopic properties as well as the nature of absorption and emission origins, the calculations were implemented using the Gaussian 03 program package[22] for complexes **1**–**5**. To save the computation time, ligand $PhP(C_2H_4PPh_2)_2$ was simplified to $HP(C_2H_4PH_2)_2$. The ground state and the lowest triplet state geometrical structures as isolated molecules in vacuum were first optimized, respectively, by the restricted and unrestricted density functional theory (DFT)[23] method with the gradient corrected correlation functional PBE1PBE.[24] During the optimization process, the convergent values of maximum force, root-mean-square (RMS) force, maximum displacement, and RMS displacement were set by default. To analyze the spectroscopic properties, 100 singlet and 6 triplet excited states were calculated, respectively, based on the optimized ground- and lowest triplet-state structures to determine the vertical excitation energies by time-dependent density functional theory (TD-DFT)[25] with the same functional used in the optimization process. In the calculation of excited states, the polarizable continuum model method (PCM)[26] using CH_2Cl_2 as the solvent was employed. The self-consistent field (SCF) convergence criterions of the RMS density matrix and maximum density matrix were set at 10^{-8} and 10^{-6} a.u., respectively, in the excited-state calculation. The iterations of excited states continue until the changes on energies of states were no more than 10^{-7} a.u. between the iterations, and then convergences were reached in all the excited states. In these calculations, the Stuttgart–Dresden (SDD)[27] basis set and the effective core potentials (ECPs) was used to describe the Au and Ag atoms. Other non-metal atoms of P, O, N, C, and H were described by the all-electron basis set of 6-31G*. Visualization of the optimized structure and frontier molecular orbitals were performed by GaussView. The Ros & Schuit method (C-squared population analysis method, SCPA)[28] was supported to analyze the partition orbital composition by using Multiwfn 2.4 program.[29]

Supporting Information

Supporting Information is available from the Wiley Online Library or from the author.

Acknowledgements

The authors are grateful for financial support from the NSFC (91122006, 21390392, 21473201, and U1405252), the 973 Project (2014CB845603) from MSTC, and the CAS/SAFEA International Partnership Program for Creative Research Teams.

Received: January 6, 2015
Revised: March 10, 2015
Published online: April 11, 2015

[1] a) W. C. H. Choy, W. K. Chan, Y. Yuan, *Adv. Mater.* **2014**, *26*, 5368; b) C. Fan, C. Yang, *Chem. Soc. Rev.* **2014**, *43*, 6439; c) P.-T. Chou, Y. Chi, *Chem. Eur. J.* **2007**, *13*, 380; d) G. Zhou, W.-Y. Wong, X. Yang, *Chem. Asian J.* **2011**, *6*, 1706; d) K. S. Yook, J. Y. Lee, *Adv. Mater.* **2012**, *24*, 3169.

[2] a) J. Kalinowski, V. Fattori, M. Cocchi, J. A. G. Williams, *Coord. Chem. Rev.* **2011**, *255*, 2401; b) A. F. Rausch, H. H. H. Homeier, H. Yersin, *Top Organomet. Chem.* **2010**, *29*, 193; c) X. Wang, Y.-L. Chang, J.-S. Lu, T. Zhang, Z.-H. Lu, S. Wang, *Adv. Funct. Mater.* **2014**, *24*, 1911; d) T. Fleetham, L. Huang, J. Li, *Adv. Funct. Mater.* **2014**, *24*, 6066; e) X. Wang, S.-L. Gong, D. Song, Z.-H. Lu, S. Wang, *Adv. Funct. Mater.* **2014**, *24*, 7257.

[3] B.-S. Du, J.-L. Liao, M.-H. Huang, C.-H. Lin, H.-W. Lin, Y Chi, H.-A. Pan, G.-L. Fan, K.-T. Wong, G.-H. Lee, P.-T. Chou, *Adv. Funct. Mater.* **2012**, *22*, 3491.

[4] a) K. M.-C. Wong, M. M.-Y. Chan, V. W.-W. Yam, *Adv. Mater.* **2014**, *26*, 5558; b) G. Cheng, K. T. Chan, W.-P. To, C.-M. Che, *Adv. Mater.* **2014**, *26*, 2540.

[5] a) M. Hashimoto, S. Igawa, M. Yashima, I. Kawata, M. Hoshino, M. Osawa, *J. Am. Chem. Soc.* **2011**, *133*, 10348; b) J. C. Deaton, S. C. Switalski, D. Y. Kondakov, R. H. Young, T. D. Pawlik, D. J. Giesen, S. B. Harkins, A. J. M. Miller, S. F. Mickenberg, J. C. Peters, *J. Am. Chem. Soc.* **2010**, *132*, 9499; c) X. Liu, T. Zhang, T. Ni, N. Jiang, Z. Liu, Z. Bian, Z. Lu, C. Huang, *Adv. Funct. Mater.* **2014**, *24*, 5385.

[6] a) W.-Y. Wong, G-J Zhou, X.-M. Yu, H.-S. Kwok, Z. Lin, *Adv. Funct. Mater.* **2007**, *17*, 315; b) E. A. Plummer, A. van Dijken, H. W. Hofstraat, L. De Cola, K. Brunner, *Adv. Funct. Mater.* **2005**, *15*, 281.

[7] a) C. Wu, H.-F. Chen, K.-T. Wong, M. E. Thompson, *J. Am. Chem. Soc.* **2010**, *132*, 3133; b) G. Nasr, A. Guerlin, F. Dumur, L. Beouch, E. Dumas, G. Clavier, F. Miomandre, F. Goubard, D. Gigmes, D. Bertin, G. Wantz, C. R. Mayer, *Chem. Commun.* **2011**, *47*, 10698.

[8] a) Q. Zhang, Q. Zhou, Y. Cheng, L. Wang, D. Ma, X. Jing, F. Wang, *Adv. Mater.* **2004**, *16*, 432; b) Q. Zhang, T. Komino, S. Huang, S. Matsunami, K. Goushi, C. Adachi, *Adv. Funct. Mater.* **2012**, *22*, 2327; c) X.-L. Chen, R. Yu, Q.-K. Zhang, L.-J. Zhou, X.-Y. Wu, Q. Zhang, C.-Z. Lu, *Chem. Mater.* **2013**, *25*, 3910; d) Q. Zhang, Q. Zhou, Y. Cheng, L. Wang, D. Ma, X. Jing, F. Wang, *Adv. Funct. Mater.* **2006**, *16*, 1203.

[9] a) K. S. Yook, J. Y. Lee, *Adv. Mater.* **2014**, *26*, 4218; b) L. Duan, L. Hou, T.-W. Lee, J. Qiao, D. Zhang, G. Dong, L. Wang, Y. Qiu, *J. Mater. Chem.* **2010**, *20*, 6392; c) C. Zhong, C. Duan, F. Huang, H. Wu, Y. Cao, *Chem. Mater.* **2011**, *23*, 326; d) X.-H. Zhu, J. Peng, Y. Cao, J. Roncali, *Chem. Soc. Rev.* **2011**, *40*, 3509.

[10] T.-W. Lee, T. Noh, H.-W. Shin, O. Kwon, J.-J. Park, B.-K. Choi, M.-S. Kim, D. W. Shin, Y.-R. Kim, *Adv. Funct. Mater.* **2009**, *19*, 1625.

[11] a) L.-J. Xu, J.-Y. Wang, L.-Y. Zhang, L.-X. Shi, Z.-N. Chen, *Organometallics* **2013**, *32*, 5402; b) I. O. Koshevoy, A. J. Karttunen, S. P. Tunik, M. Haukka, S. I. Selivanov, A. S. Melnikov, P. Y. Serdobintsev, T. A. Pakkanen, *Organometallics* **2009**, *28*, 1369; c) I. O. Koshevoy, Y.-C. Lin, A. J. Karttunen, P.-T. Chou, P. Vainiotalo, S. P. Tunik, M. Haukka, T. A. Pakkanen, *Inorg. Chem.* **2009**, *48*, 2094; d) L.-Y. Zhang, L.-J. Xu, X. Zhang, J.-Y. Wang, J. Li, Z.-N. Chen, *Inorg. Chem.* **2013**, *52*, 5167.

[12] Y. Ma, C.-M. Che, H.-Y. Chao, X. Zhou, W.-H. Chan, J. Shen, *Adv. Mater.* **1999**, *11*, 852.

[13] T. M. Dau, Y.-A. Chen, A. J. Karttunen, E. V. Grachova, S. P. Tunik, K.-T. Lin, W.-Y. Hung, P.-T. Chou, T. A. Pakkanen, I. O. Koshevoy, *Inorg. Chem.* **2014**, *53*, 12720.

[14] a) Z.-H. Chen, L.-Y. Zhang, Z.-N. Chen, *Organometallics* **2012**, *31*, 256; b) D. Fernandez-Anca, M. I. Garcia-Seijo, A. Castineiras, M. E. Garcia-Fernandez, *Inorg. Chem.* **2008**, *47*, 5685.

[15] B. S. Kim, J. Y. Lee, *Adv. Funct. Mater.* **2014**, *24*, 3970.

[16] a) Y.-S. Park, S. Lee, K.-H. Kim, S.-Y. Kim, J.-H. Lee, J.-J. Kim, *Adv. Funct. Mater.* **2013**, *23*, 4914; b) M. Cai, T. Xiao, E. Hellerich, Y. Chen, R. Shinar, J. Shinar, *Adv. Mater.* **2011**, *23*, 3590.

[17] Y. Tao, C. Yang, J. Qin, *Chem. Soc. Rev.* **2011**, *40*, 2943.

[18] a) A. Perumal, H. Faber, N. Yaacobi-Gross, P. Pattanasattayavong, C. Burgess, S. Jha, M. A. McLachlan, P. N. Stavrinou, T. D. Anthopoulos, D. D. C. Bradley, *Adv. Mater.* **2015**, *27*, 93; b) P. Pattanasattayavong, N. Yaacobi-Gross, K. Zhao, G. O. N. Ndjawa, J. Li, F. Yan, B. C. O'Regan, A. Amassian, T. D. Anthopoulos, *Adv. Mater.* **2013**, *25*, 1504; c) P. Pattanasattayavong, G. O. N. Ndjawa, K. Zhao, K. W. Chou, N. Yaacobi-Gross, B. C. O'Regan, A. Amassian, T. D. Anthopoulos, *Chem. Commun.* **2013**, *49*, 4154.

[19] a) W. E. Hill, J. G. Taylor, C. A. McAuliffe, K. W. Muir, L. M. Muir, *J. Chem. Soc. Dalton Trans.* **1982**, 833; b) D. C. Owsley, C. E. Castro, *Org. Synth.* **1972**, *52*, 128.

[20] J. N. Demasa, G. A. Crosby, *J. Phys. Chem.* **1971**, *75*, 991.

[21] G. M. Sheldrick, *SHELXL-97, Program for the Refinement of Crystal Structures*, University of Göttingen, Göttingen, Germany **1997**.

[22] M. J. Frisch, G. W. Trucks, H. B. Schlegel, G. E. Scuseria, M. A. Robb, J. R. Cheeseman, J. A. Montgomery Jr., T. Vreven, K. N. Kudin, J. C. Burant, J. M. Millam, S. S. Iyengar, J. Tomasi, V. Barone, B. Mennucci, M. Cossi, G. Scalmani, N. Rega, G. A. Petersson, H. Nakatsuji, M. Hada, M. Ehara, K. Toyota, R. Fukuda, J. Hasegawa, M. Ishida, T. Nakajima, Y. Honda, O. Kitao, H. Nakai, M. Klene, X. Li, J. E. Knox, H. P. Hratchian, B. J. Cross, V. Bakken, C. Adamo, J. Jaramillo, R. Gomperts, R. E. Stratmann, O. Yazyev, A. J. Austin, R. Cammi, C. Pomelli, J. W. Ochterski, P. Y. Ayala, K. Morokuma, G. A. Voth, P. Salvador, J. J. Dannenberg, V. G. Zakrzewski, S. Dapprich, A. D. Daniels, M. C. Strain, O. Farkas, D. K. Malick, A. D. Rabuck, K. Raghavachari, J. B. Foresman, J. V. Ortiz, Q. Cui, A. G. Baboul, S. Clifford, J. Cioslowski, B. B. Stefanov, G. Liu, A. Liashenko, P. Piskorz, I. Komaromi, R. L. Martin, D. J. Fox, T. Keith, M. A. Al-Laham, C. Y. Peng, A. Nanayakkara, M. Challacombe, P. M. W. Gill, B. Johnson, W. Chen, M. W. Wong, C. Gonzalez, J. A. Pople, Gaussian 03, revision D.02, Gaussian, Inc., Wallingford, CT **2004**.

[23] A. D. Becke, *J. Chem. Phys.* **1993**, *98*, 5648.

[24] J. P. Perdew, K. Burke, M. Ernzerhof, *Phys. Rev. Lett.* **1996**, *77*, 3865.

[25] a) M. E. Casida, C. Jamorski, K. C. Casida, D. R. Salahub, *J. Chem. Phys.* **1998**, *108*, 4439; b) R. E. Stratmann, G. E. Scuseria, M. J. Frisch, *J. Chem. Phys.* **1998**, *109*, 8218; c) R. Bauernschmitt, R. Ahlrichs, *Chem. Phys. Lett.* **1996**, *256*, 454.

[26] a) V. Barone, M. Cossi, J. Tomasi, *J. Chem. Phys.* **1997**, *107*, 3210; b) M. Cossi, G. Scalmani, N. Rega, V. Barone, *J. Chem. Phys.* **2002**, *117*, 43.

[27] a) M. Dolg, U. Wedig, H. Stoll, H. Preuss, *J. Chem. Phys.* **1987**, *86*, 866; b) P. Schwerdtfeger, M. Dolg, W. H. E. Schwarz, G. A. Bowmaker, P. D. W. Boyd, *J. Chem. Phys.* **1989**, *91*, 1762; c) D. Andrae, U. Häussermann, M. Dolg, H. Stoll, H. Preuss, *Theor. Chim. Acta* **1990**, *77*, 123.

[28] P. Ros, G. C. A. Schuit, *Theor. Chim. Acta* **1966**, *4*, 1.

[29] T. Lu, F. W. Chen, *J. Comp. Chem.* **2012**, *33*, 580.